Bulletin of Mathematical Biology (2002) **64**, 261–284
doi:10.1006/bulm.2001.0273
Available online at http://www.idealibrary.com on IDEAL®

Home Range Formation in Wolves Due to Scent Marking

BRIAN K. BRISCOE, MARK A. LEWIS* AND STEPHEN E. PARRISH
Department of Mathematics,
University of Utah,
Salt Lake City,
UT 84112,
U.S.A.
E-mails: briscoe@math.utah.edu; mlewis@math.ualberta.ca; parrish@math.utah.edu

Social carnivores, such as wolves and coyotes, have distinct and well-defined home ranges. During the formation of these home ranges scent marks provide important cues regarding the use of space by familiar and foreign packs. Previous models for territorial pattern formation have required a den site as the organizational center around which the territory is formed. However, well-defined wolf home ranges have been known to form in the absence of a den site, and even in the absence of surrounding packs. To date, the quantitative models have failed to describe a mechanism for such a process. In this paper we propose a mechanism. It involves interaction between scent marking and movement behavior in response to *familiar* scent marks. We show that the model yields distinct home ranges by this new means, and that the spatial profile of these home ranges is different from those arising from the territorial interactions with den sites.

© *2002 Society for Mathematical Biology*

1. INTRODUCTION

Field biologists have observed wolves and coyotes using scent marks to identify home ranges and territories (defended home ranges) (Mech, 1991). Canids can distinguish between a foreign scent mark and one of their own (Peters, 1974; Merti-Millhollen *et al*., 1986) and, when encountering a foreign scent mark, may mark over it (Peters and Mech, 1975). Foreign scent marks may also elicit an avoidance response, with individuals exhibiting an increased probability of moving towards the center of their home range (Peters and Mech, 1975). Continuum territory models, based on the above elements of behavior, have been proposed by Lewis and Murray (1993) and others (Lewis *et al*., 1997; White *et al*., 1996, 1998; Moorcroft *et al*., 1999), and can be derived from random walks, as shown in Moorcroft *et al*. (1999). Together the models address how the interaction between scent marking and movement behavior in response to foreign scent marks can lead to territorial

*Author to whom correspondence should be addressed. Department of Mathematical and Statistical Sciences, LAB 545 B, University of Alberta, Edmonton, Alberta T6G 2G1, Canada.

0092-8240/02/020261 + 24 $35.00/0 © 2002 Society for Mathematical Biology

patterns. In these models a den site acts as a focal point for the movement of individuals and this focal point is a necessary element of the model if territories are to form (White *et al*., 1996).

However, well-defined wolf home ranges have been known to form in the absence of a den site (Rothman and Mech, 1979), and even in the absence of surrounding packs (Mech, 1991). To date, the quantitative models have failed to describe a mechanism for this process. In this paper we propose a mechanism for the process. It involves interaction between scent marking and movement behavior in response to *familiar* scent marks. We show that the model yields distinct home ranges by this new means, and that the spatial profile of these home ranges is distinct from those arising from the territorial interactions with den sites present.

Our modeling approach is to describe the change in the location of an individual via a random walk process. This leads to a coupled partial differential equation (PDE)/ordinary differential equation (ODE) model through the limiting processes of the random walk. The modeling approach is outlined in Aronson (1985) and has been applied widely (Okubo, 1980). Two applications relevant to this paper include modeling of aggregating insect populations by Turchin (1989), and the modeling of aggregating populations with long-range interactions between individuals by Lewis (1994).

In our model formulation it is assumed that the pack is initially isolated, with no neighboring packs, and no established den site. Individuals both produce scent marks and modify their movement behavior in response to their pack's scent marks. The model, described as a 'random walk' process, assumes that the transition probabilities describing spatial movement depend upon the local level of scent marks, and that scent mark production also depends upon existing scent marks.

Analysis of the coupled ODE/PDE system shows spontaneous formation of well-defined home ranges for reasonable parameter ranges. These home ranges have abrupt edges and are stable to perturbations. Energy methods and numerical methods are used to calculate the home range patterns. The results in this paper contrast with previous model results where *foreign* scent marks and a den site are necessary ingredients for the process of territorial pattern formation (Lewis and Murray, 1993; White *et al*., 1996; Moorcroft *et al*., 1999).

2. Model Derivation

We first consider a derivation in one spatial dimension, and then we extend this to a two-dimensional (2D) model.

2.1. ***One-dimensional approach.*** A classical approach to deriving a PDE model, based on the movement of an individual comes from a random walk on the real line (Okubo, 1980). In our formulation, we assume that an individual's movement behavior is modulated by local scent density—individuals preferentially remain in

areas with high scent levels. We begin the random walk derivation by discretizing both time and space into small intervals of length δt and δx, respectively. We assume that each individual at each point in time decides whether or not to move, and if so, in which direction. We also assume that an individual can only move a distance of δx, or remain in its current position in each successive time step, δt. We let $L(x,t)$, $R(x,t)$ and $N(x,t)$ be the probabilities of moving to the left, to the right, and of not moving, respectively, over the next time step. Taking these as the only possibilities, we have that

$$N(x,t) + L(x,t) + R(x,t) = 1. \tag{1}$$

If scent level is high, $N(x,t)$ is close to 1, and the wolf tends not to move, however if scent levels are low, $N(x,t)$ is small, and the individual is more likely to move. If we make the assumption that a wolf moves depending only on the scent level at its present location, it is logical to take $L(x,t) = R(x,t)$. Combining this with (1) we get

$$L(x,t) = R(x,t) = \frac{1 - N(x,t)}{2}. \tag{2}$$

The forward Kolmogorov, or Fokker–Planck equation, relates these probabilities to the following PDE:

$$\frac{\partial u}{\partial t} = D_0 \frac{\partial^2}{\partial x^2}[(1 - N(x,t))u(x,t)] \tag{3}$$

where $u(x,t)$ is the expected population density. Details of the derivation are given in Appendix A. However we note here that $D_0 = \lim_{\delta x, \delta t \to 0} \delta x^2 / 2\delta t$ is the diffusion coefficient, which is derived under the assumption of rapid movement and frequent switches in movement direction. For simplicity, we can make the substitution

$$D(x,t) = D_0(1 - N(x,t)), \tag{4}$$

which brings us to

$$\frac{\partial u}{\partial t} = \frac{\partial^2}{\partial x^2}[D(x,t)u(x,t)]. \tag{5}$$

Now, turning our attention to the scent marking equation, we make some simple, biologically relevant assumptions. We define $p(x,t)$ to be the density of scent marks. First of all, we assume that wolves mark with scent at a constant rate, γ, but increase the marking rate when they encounter scent marks other than their own. The increasing function $m(p)$ describes enhanced scent mark rates in the presence of existing scent marks. Finally, it is assumed that scent marks decay with time at a constant rate, μ. The equation for scent is then

$$\frac{\partial p}{\partial t} = u(x,t)(\gamma + m(p(x,t))) - \mu p(x,t). \tag{6}$$

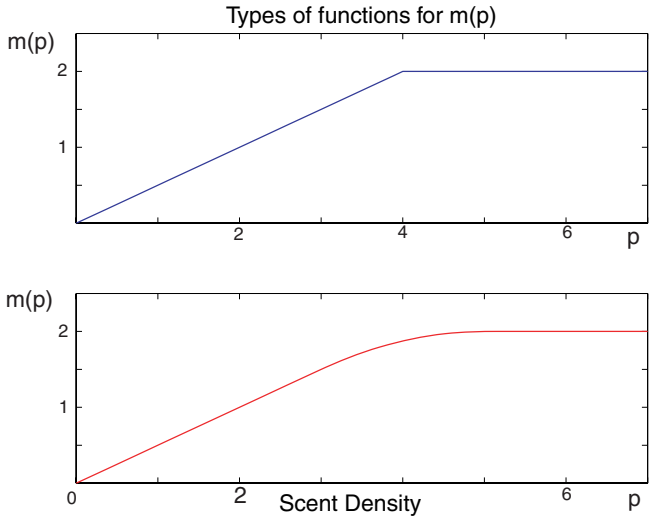

Figure 1. This shows the two possible scent-response functions, $m(p)$, that we use. The top figure is the piecewise linear, and the bottom is the piecewise quadratic, found in Appendix B.

The first form we consider for $m(p)$ gives the simplest type of response, linear increase up to some level of $p(x,t)$, at which the response becomes constant, as in the first graph of Fig. 1. The second form is similar, but it is piecewise quadratic, as in the second graph of Fig. 1.

We assume that the probability of not moving, $N(x,t)$, increases monotonically with scent density $p(x,t)$. In the absence of detailed data on the precise relationship between $N(x,t)$ and $p(x,t)$ we take this to be

$$N(x,t) = \frac{p(x,t)}{\alpha + p(x,t)}. \tag{7}$$

The parameter α describes the sensitivity of movement behavior to scent mark levels when scent mark levels are low. Using this and equation (4), we can find an explicit expression for $D(x,t)$

$$D(x,t) = \frac{D_0}{1 + p(x,t)/\alpha}. \tag{8}$$

Our system of equations is now fully defined as

$$\frac{\partial u}{\partial t} = \frac{\partial^2}{\partial x^2}\left(\frac{D_0 u}{1 + p/\alpha}\right), \tag{9}$$

$$\frac{\partial p}{\partial t} = u(\gamma + m(p)) - \mu p. \tag{10}$$

In our analyses we will assume a domain $0 < x < L$ from which the wolves do not leave and hence zero-flux boundary conditions,

$$\frac{\partial}{\partial x}\left(\frac{D_0 u}{1 + p/\alpha}\right) = 0 \qquad \text{at} \qquad x = 0, L, \tag{11}$$

are appropriate.

2.2. ***Two spatial dimensions.*** As much insight as a one-dimensional model can give us, it falls short of reality. In their natural environment, wolves move over two dimensions. Our 2D derivation uses a similar approach to the one in the previous section. Once again, we begin with a random walk, but this time we add another degree of freedom. As before, we let $L(\mathbf{x}, t)$, $R(\mathbf{x}, t)$ and $N(\mathbf{x}, t)$ be the probabilities of moving to the left, to the right and not moving, respectively. We then add to these the possibilities of moving forward and backward, which we will denote with $F(\mathbf{x}, t)$ and $B(\mathbf{x}, t)$. It is also important to note that these values now depend on two spatial parameters, and therefore $\mathbf{x} = (x_1, x_2)$. Taking these as the only possibilities, we have

$$N(\mathbf{x}, t) + R(\mathbf{x}, t) + L(\mathbf{x}, t) + F(\mathbf{x}, t) + B(\mathbf{x}, t) = 1. \tag{12}$$

If we assume a wolf's decision to move only depends on his current position, we can also assume that

$$R(\mathbf{x}, t) = L(\mathbf{x}, t) = F(\mathbf{x}, t) = B(\mathbf{x}, t) = \frac{1 - N(\mathbf{x}, t)}{4}. \tag{13}$$

A derivation analogous to the one in the previous section yields a system of equations similar to the one-dimensional (1D) case.

$$\frac{\partial u}{\partial t} = \Delta\left(\frac{D_0 u}{1 + p/\alpha}\right) \tag{14}$$

$$\frac{\partial p}{\partial t} = u(\gamma + m(p)) - \mu p, \tag{15}$$

on the solution domain Ω (Parrish, 1998) where now $D_0 = \lim_{\delta x, \delta_t \to 0} \delta x^2 / 4\delta t$. Zero flux boundary conditions become

$$\nabla\left(\frac{D_0 u}{1 + p/\alpha}\right) \cdot \mathbf{n} = 0 \tag{16}$$

on the boundary $\delta\Omega$, where $\mathbf{n}$ is the outwardly-oriented unit normal vector.

3. A NONLOCAL APPROXIMATION

In the previous equation for the scent, we assumed that the level of an individual's response depends only on local scent densities. This is not realistic however, because wolves can indeed sense scent markings at a distance (Peters, 1974) We now take into consideration how scent markings that are near the position of an individual wolf play a role in the wolf's decision-making.

Let $k(x)$ be a symmetric, olfactory kernel which integrates to unity and defines the locally averaged scent mark density by

$$\int_{-\infty}^{\infty} k(z-x)\,p(z,t)\,dz. \tag{17}$$

This can be approximated by

$$\overline{p}(x,t) = p(x,t) + \frac{\sigma^2}{2}\frac{\partial^2}{\partial x^2}p(x,t) \tag{18}$$

where σ^2 is the second moment of the olfactory kernel k, a measure of its variance or spread (Murray, 1989). When decisions are made based on the locally averaged scent mark density, $\bar{p}$ can replace p in equation (9) and in the function m in equation (10). To keep our analysis analytically tractable, we only consider the case where $m(\bar{p})$ is used in equation (10), with $\sigma^2 \geq 0$. This change leads us to a new scent marking equation:

$$\frac{\partial p}{\partial t} = u(\gamma + m(\overline{p}(x,t))) - \mu p. \tag{19}$$

We will show that $\sigma^2 > 0$ is required to ensure that (9), (10) are well posed.

3.1. ***Two-dimensional approximation.*** In two spatial dimensions, the analysis yields an analogous result, with

$$\overline{p}(\mathbf{x},t) = p(\mathbf{x},t) + \frac{\sigma^2}{2}\Delta p(\mathbf{x},t). \tag{20}$$

Substituting this into (15), we have an equation identical to (19) where x is now a 2D spatial coordinate.

It should be noted that in the limit $\sigma = 0$ the kernel k corresponds to a delta distribution centered at the wolf's current position, so that only local scent densities are taken into consideration. In this case (19) is simplified to (10) or (15).

4. ANALYSIS OF EQUATIONS

4.1. ***Nondimensionalization.*** Before doing any analysis, we nondimensionalize (9) and (19) in order to reduce the number of parameters. It is possible to reduce the number of parameters by four since there are four variables: u, p, t and x. The nondimensional variables are

$$\hat{x} = \frac{x}{L}, \qquad \hat{t} = \frac{\mu}{\epsilon}t, \qquad \epsilon = \frac{D_0}{\mu L^2}, \qquad \hat{u} = \frac{\gamma u}{\alpha\mu}, \qquad \hat{p} = \frac{p}{\alpha}, \qquad \hat{\sigma} = \frac{\sigma}{L}.$$

After making the aforementioned substitutions and dropping the carets, the nondimensional equations are

$$\frac{\partial u}{\partial t} = \frac{\partial^2}{\partial x^2}\left(\frac{u}{1+p}\right), \tag{21}$$

$$\epsilon\frac{\partial p}{\partial t} = \frac{u}{\gamma}(\gamma + m(\alpha\overline{p})) - p, \tag{22}$$

with boundary conditions

$$\frac{\partial}{\partial x}\left(\frac{u}{1+p}\right) = 0 \qquad \text{at} \quad x = 0, 1. \tag{23}$$

The parameter ϵ is small when the domain is large relative to spreading due to local diffusion over the characteristic time scale μ^{-1}.

An analogous 2D nondimensionalization can be used for (14), (19) to yield

$$u_t = \Delta\left(\frac{u}{1+p}\right), \tag{24}$$

$$\epsilon\frac{\partial p}{\partial t} = \frac{u}{\gamma}(\gamma + m(\alpha\overline{p})) - p, \tag{25}$$

on Ω with boundary condition

$$\nabla\left(\frac{u}{1+p}\right)\cdot\mathbf{n} = 0 \qquad \text{on} \quad \partial\Omega. \tag{26}$$

Note that the total number of wolves U_0 is conserved because

$$\frac{d}{dt}\int_\Omega u\,dx = \int_\Omega \nabla\cdot\nabla\left(\frac{u}{1+p}\right)dx = \int_{\delta\Omega}\nabla\left(\frac{u}{1+p}\right)\cdot\mathbf{n}\,ds = 0. \tag{27}$$

4.2. ***Steady state solutions.*** We now focus on analysis of the 1D spatial system, (21)–(23), while noting that analysis of the analogous 2D system, (24)–(26), is similar. Steady state solutions to (21), (22) satisfy

$$\frac{\partial^2}{\partial x^2}\left(\frac{u}{1+p}\right) = 0, \tag{28}$$

$$\frac{u}{\gamma}(\gamma + m(\alpha\bar{p})) - p = 0. \tag{29}$$

Application of the zero flux boundary conditions (23) yields

$$\frac{u}{1+p} = \text{const.}$$

If the steady state solution is spatially homogeneous or if $\sigma^2 = 0$, then

$$\frac{u}{\gamma}(\gamma + m(\alpha p)) - p = 0.$$

Solving this equation for $p = f(u)$ yields

$$\frac{u}{1+f(u)} = \text{const} \tag{30}$$

(Fig. 2). Details are given in Appendix C. We observe that, depending upon the value of the constant, there will be one, two or three values of u satisfying (30). We define

$$\phi(u) = \frac{u}{1+f(u)} - C, \tag{31}$$

where C is chosen to be the unique constant that ensures

$$\int_{u_1^*}^{u_3^*} \phi(u)\,du = 0, \tag{32}$$

and u_1^* and u_3^* are the left and rightmost roots of ϕ as shown in Fig. 3. This shift in (31) by a constant will aid the subsequent graphical analysis.

At steady state, (28) becomes

$$\frac{\partial^2}{\partial x^2}(\phi(u)) = 0, \tag{33}$$

which has the solution

$$\phi(u) = \lambda \quad \text{(constant)}. \tag{34}$$

A steady state solution u_s, satisfying (34) for some λ, has a corresponding scent mark level $p_s = f(u_s)$.

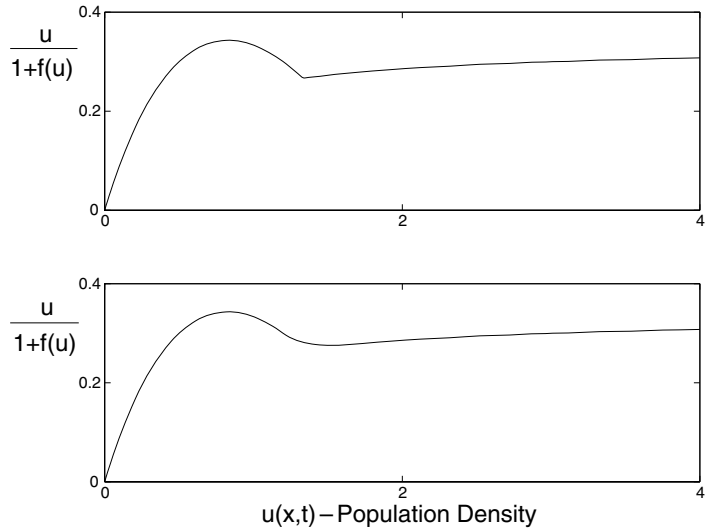

Figure 2. These are the functions $u/(1 + f(u))$ associated with $m(p)$ in Fig. 1. The equations for these functions are found in Appendix C.

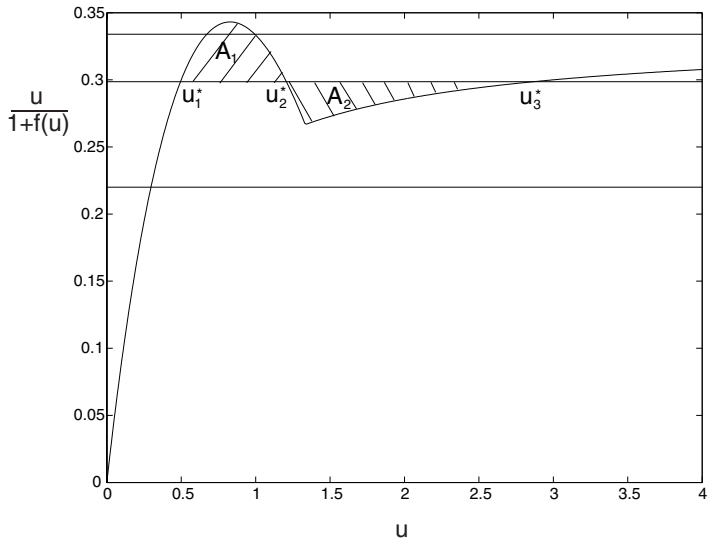

Figure 3. This is the top function from Fig. 2, which is simply $u/(1 + f(u))$, along with three different constants as in (30). The middle constant is the unique value given in (31), $C = 0.299$, which satisfies (32), i.e., the constant which makes $A_1 = A_2$. The values of u_1^*, u_2^* and u_3^* are 0.495, 1.21 and 2.86, respectively.

4.3. ***Dispersion relation.*** To analyze the stability of a spatially homogeneous steady state solution (u_s, p_s) we linearize, with $u = u_s + v$ and $p = p_s + q$, where $|v|, |q| \ll 1$. Substitution into (21), (22) yields the linearized system

$$\frac{\delta v}{\delta t} \approx \left(\frac{v_{xx}}{1+p_s} - \frac{u_s q_{xx}}{(1+p_s)^2} \right), \tag{35}$$

$$\epsilon \frac{\delta q}{\delta t} \approx \left(u_s \left(\frac{m'(p_s)}{\gamma} q + \frac{\sigma^2}{\gamma} m'(p_s) q_{xx} \right) - q \right) + v \left(1 + \frac{m(p_s)}{\gamma} \right). \tag{36}$$

If we consider solutions of the form

$$\hat{w} = \begin{pmatrix} v(x,t) \\ q(x,t) \end{pmatrix} = e^{st+ikx} \begin{pmatrix} v_0 \\ q_0 \end{pmatrix}, \tag{37}$$

then substitute $\hat{w}$ into (35) and (36), we have

$$s\hat{w} = \begin{pmatrix} \frac{-k^2}{1+p_s} & \frac{u_s k^2}{(1+p_s)^2} \\ \frac{1}{\epsilon}\left(1 + \frac{m(p_s)}{\gamma}\right) & \frac{1}{\epsilon}\left(\frac{u_s m'(p_s)}{\gamma}(1-\sigma^2 k^2) - 1\right) \end{pmatrix} \hat{w} = A\hat{w}. \tag{38}$$

This is the eigenvalue equation for the matrix A. For the equation to be satisfied for a nontrivial value, we require $\det(A - sI) = 0$. This gives a characteristic polynomial, which can be solved for s in terms of the wavenumber k. We will also allow σ^2 to vary to see what effect it has on pattern formation. By looking at (37), we observe that the wavenumbers k that correspond to $s > 0$ will grow with wavelength $2\pi/k$.

Figure 4 shows the dispersion relation for $(u_s, p_s) = (u_2^*, f(u_2^*)) = (1.21, 3.04)$ for the cases where $\sigma = 0$ and $\sigma = 0.01$. Note that this u_s is found on the descending (middle) branch of ϕ [i.e., $\phi'(u_2^*) < 0$]. [See Section 4.2, equation (C1) in Appendix C, and Fig. 3.] Figure 5 shows the same dispersion relation for $0 \leq \sigma \leq 0.1$. For the case $\sigma = 0$, the dispersion relation increases monotonically, and hence the smallest wavelength perturbations grow the fastest. This is the hallmark of an ill-posed problem. From a modeling perspective, we observe that this comes from the random walk process when all scent mark information, however close by, is ignored, except the scent density immediately under the individual wolf. This problem is corrected if there is any spatial averaging of scent mark information ($\sigma > 0$). In this case, $s > 0$ over a range of wavenumbers indicates that spatial patterns may form spontaneously from the spatially homogeneous solution.

5. AN ENERGY METHOD

As mentioned in Section 4.2, equation (34) can have either one, two or three solutions, depending on the value of λ. This raises the question as to whether

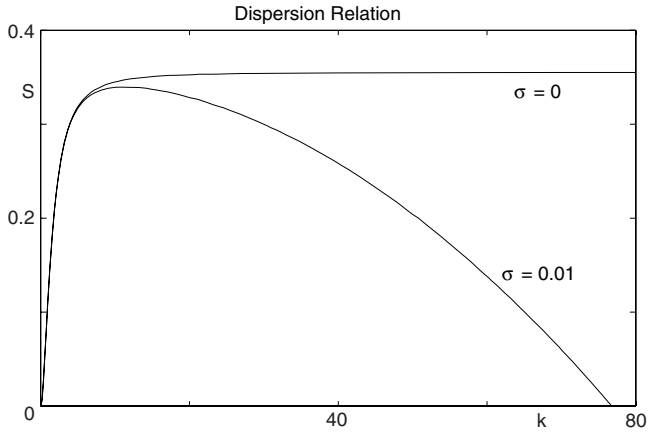

Figure 4. This is the dispersion relation when $\sigma = 0, 0.01$. The first is a bounded, increasing function for $k^2 > 0$. Because of this, the high wavenumbers (small wavelengths) grow the fastest. The second increases until it attains a maximum value, and then decreases and becomes negative. In this case, there is a finite range of wavenumbers that will grow.

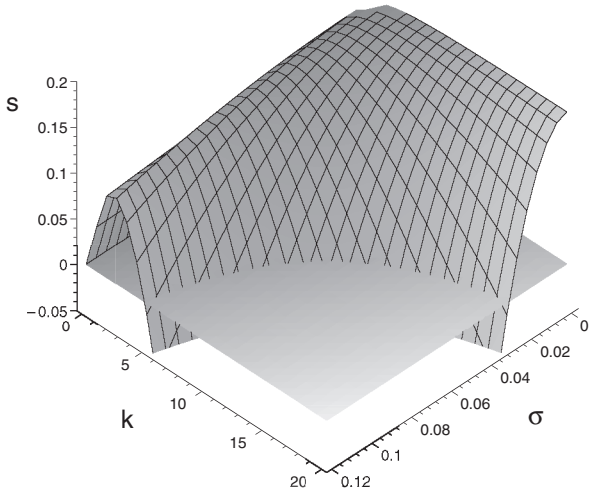

Figure 5. This is the dispersion relation plotted against σ and k for the system we have been analyzing along with the plane $s = 0$. Recall for $s > 0$, the area which is above the plane $s = 0$, perturbations of the corresponding wavelength will grow.

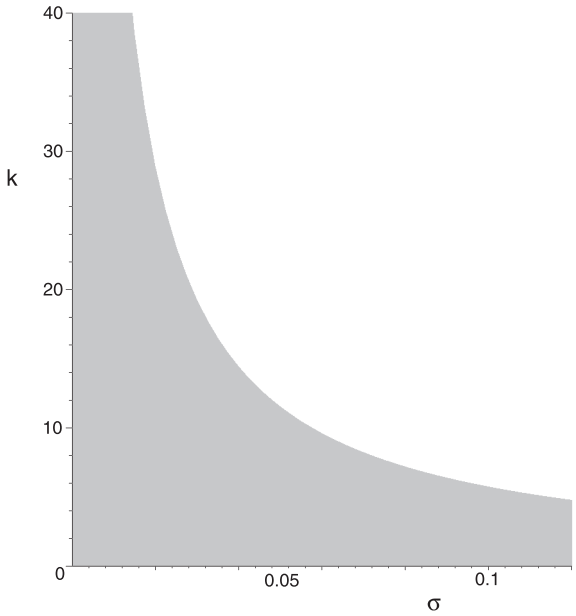

Figure 6. The curve plotted here is where the dispersion relation is zero. The values of σ and k in the shaded region correspond to growing perturbations, whereas the values above the curve lead to decaying perturbations. If we choose a particular value of σ, we can now find the range of wavelengths that will grow. See, also, Figs 4 and 5.

spatially heterogeneous discontinuous solutions may exist for (21), (22) in the limit as $\sigma \to 0$, where $u = u_1$ on measure L_1, $u = u_2$ on measure L_2 and $u = u_3$ on measure $L_3 = 1 - L_1 - L_2$. We investigate this question using an energy method and focus on the case where the domain size is large ($\epsilon \to 0$). Using this method we will show that, providing the total number of wolves U_0 is sufficiently large, the lowest energy solution is $L_2 = 0$ and $u = u_1$ on an interval of length L_1 and $u = u_3$ on an interval $1 - L_1$, where L_1 is found by solving $u_1 L_1 + (1 - L_1)u_3 = U_0$. The region over which $u = u_3$ is the home range. See, for example, Fig. 12.

5.1. ***Defining the energy.*** We define our energy to be a quantity which is bounded below, and show that it is a decreasing function of time.

The first thing we might wish to do is consider the case where $\epsilon \ll 1$. This is reasonable because, in our nondimensionalization, $\epsilon = D_0/(\mu L^2)$. In realistic cases, L can be chosen so that $L^2 \gg D_0$ and μ is of order 1. This reduces (21), (22) to

$$\frac{\partial u}{\partial t} = \frac{\partial^2}{\partial x^2}(\phi(u)), \tag{39}$$

where ϕ is defined in (31).

We define our energy to be

$$E(u) = \int_0^1 F(u(x,t))\,dx, \tag{40}$$

where $F'(u) = \phi(u)$, and observe that

$$\dot{E}(u) = \int_0^1 F'(u)\frac{\partial u}{\partial t}(x)\,dx = \int_0^1 F'(u)[\phi(u)]_{xx}\,dx. \tag{41}$$

Integrating (41) by parts and using the boundary condition (11) to eliminate the boundary term yields

$$\dot{E}(u) = -\int_0^1 \frac{\partial}{\partial x}(F'(u))\frac{\partial}{\partial x}[\phi(u)]\,dx = -\int_0^1 \left(\frac{\partial}{\partial x}[\phi(u)]\right)^2 dx \leq 0. \tag{42}$$

As long as the flux, $\frac{\partial}{\partial x}\phi(u)$, is nonzero, $E(u)$ will decrease with time. Also, since $\phi(u)$ is a bounded function, the energy, $E(u)$ is bounded below for $u \geq 0$. This prompts us to look for a global minimum for the energy, (40).

5.2. ***Minimizing the energy.*** To minimize $E(u)$, we will use Lagrange multipliers and constraint (27). We define

$$L(u) = \int_0^1 F(u)\,dx - \lambda\int_0^1 (u - U_0)\,dx, \tag{43}$$

which is the quantity to be minimized. If we assume that u minimizes this equation, and $u + \delta\eta(x)$ is a variation, then a minimum of $L(u + \delta\nu(x))$ should occur when $\delta = 0$. Taking the derivative with respect to δ we get

$$L_\delta = \int_0^1 (F'(u + \delta\eta(x))\eta(x) - \lambda\eta(x))\,dx \tag{44}$$

evaluating this at $\delta = 0$ we get

$$L_\delta = \int_0^1 (F'(u)\eta(x) - \lambda\eta(x))\,dx \tag{45}$$

$$L_\delta = \int_0^1 (F'(u) - \lambda)\eta(x)\,dx. \tag{46}$$

Since $\eta(x)$ is an arbitrary function, the minimum energy occurs precisely when $F'(u) = \lambda$ which, when substituting $F'(u) = \phi(u)$, gives us the same condition as (34): $\phi(u) = \lambda$. From equation (42) we observe that $\phi(u) = \lambda$ implies that E

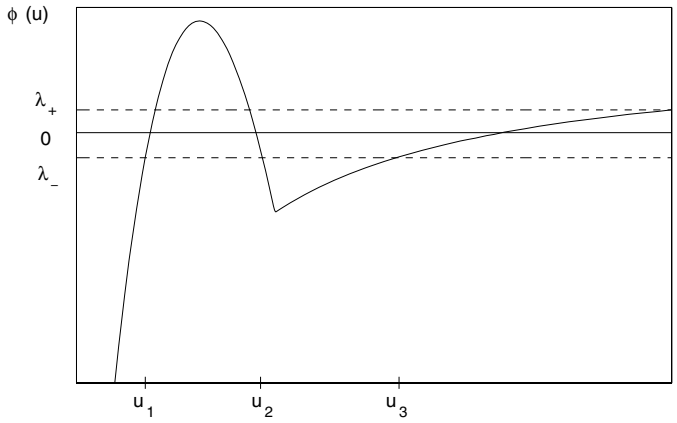

Figure 7. This a plot of $\phi(u)$ as defined in (31) and plotted in Fig. 3. As mentioned, (34) can hold for any constant. The solid line is $\lambda = 0$. The values u_1, u_2, and u_3 correspond to $\phi(u) = \lambda_-$. With both constants shown, the solution to (34) has three solutions, however, it is also possible to find constants such that (34) has one or two solutions as well (Fig. 2).

is no longer decreasing ($\dot{E} = 0$). We now consider which value of λ will give a global minimum for the energy (40).

We consider the cases shown in Fig. 7, where three distinct values of u satisfy (34), and observe that (40) becomes

$$E(u) = \sum_{i=1}^{N} L_i F(u_i), \tag{47}$$

where

$$\sum_{i=1}^{N} L_i = 1, \tag{48}$$

and N is the number of distinct solutions to (34). Using (47) and (48) we find that the energy equation reduces to a convex combination of $F(u_i)$. When $N = 3$, we have that

$$E(u) = L_1 F(u_1) + L_2 F(u_2) + (1 - L_1 - L_2) F(u_3) \tag{49}$$

We have one more constraint given in (27) which is

$$U = \sum_{i=1}^{N} L_i u_i = U_0, \tag{50}$$

where U_0 is the normalized total number of wolves. For the case $N = 3$, the choice of L_1 and L_2 to give the minimum value for $E(u)$ (49) has been analyzed in detail by Parrish (1998). Here we give a simple graphical argument. First we observe

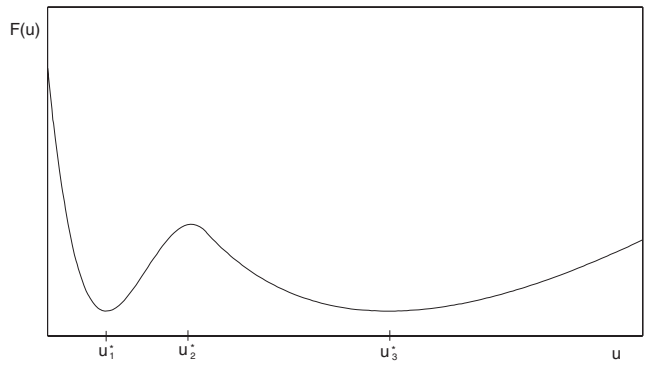

Figure 8. This is the function $F(u)$ defined in Section 5.1. As given in Fig. 3, the values of u_1^*, u_2^* and u_3^* are 0.495, 1.21 and 2.86, respectively.

that the function F corresponding to ϕ (Fig. 3), where $F'(u) = \phi(u)$, has the form shown in Fig. 8.

Now for any L_1 and L_2 ($0 \leq L_1 + L_2 \leq 1$) the total population number U (50) and the energy E (49) are depicted graphically as the coordinates of a point in the triangle whose vertices are $[u_1, F(u_1)]$, $[u_2, F(u_2)]$ and $[u_3, F(u_3)]$ (Figs 9–11). In Fig. 9, the points u_1, u_2 and u_3 are chosen so that $\phi(u_1) = \phi(u_2) = \phi(u_3) = \lambda_+ > 0$ (Fig. 7, upper line), and hence $F'(u_1) = F'(u_2) = F'(u_3) = \lambda_+ > 0$ (Fig. 9). The constraint $U = U_0$ (50) is depicted by the vertical line segment in Fig. 9, and the minimum possible energy, given that $U = U_0$, ($E_{\min}$) comes at the point where the vertical line segment touches the base of the triangle.

The cases $\lambda < 0$ and $\lambda = 0$ are shown in Figs 10 and 11. Thus the lowest possible energy comes from the case $\lambda = 0$ where $u_1 = u_1^*$, $u_2 = u_2^*$ and $u_3 = u_3^*$ (compare Figs 9, 10 and 11). For this case, $u_1 = 0.495$, $u_2 = 1.21$ and $u_3 = 2.86$. Using (48) and (50) we find that $L_1 = 0.787$ and $L_3 = 0.213$.

Our analysis has shown that when $\sigma, \epsilon \to 0$, the energy of the system will decrease until $\phi(u) = \lambda$(const). Each value of λ defines a u_3 value (within home range density) and a u_1 value (outside home range density) and the low-energy solution has measure L_1 outside of the home range $u = u_1$ and measure $1 - L_1$ within the home range $u = u_3$. The value of λ which gives the global energy minimum (minimum over all possible λ) is $\lambda = 0$, with corresponding within home range density and outside home range density given by u_3^* and u_1^*, respectively. We now use numerical simulation to see whether the global energy minimum is achieved.

6. Numerical Solutions of the System

Numerical simulations used a finite difference, Crank–Nicolson method with variable weighting between forward and backward differencing in time for each equation. For computational simplicity, equation (22) was solved using forward

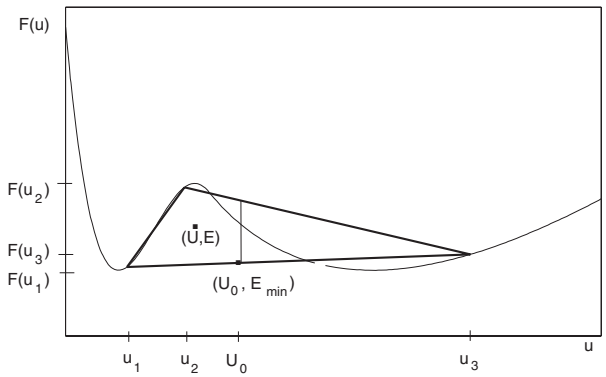

Figure 9. This represents the function $F(u)$, plotted against u. The triangle is the convex combination of $F(u_1)$, $F(u_2)$ and $F(u_3)$, where $\lambda = \lambda_+ > 0$ and an arbitrary energy value is shown. The energy associated with a particular U_0 is somewhere along the vertical line, and is clearly minimized at the bottom of the vertical line. This implies that at the minimum energy level, steady state solutions consist only of the values of u_1 and u_3, and u_2 is unstable.

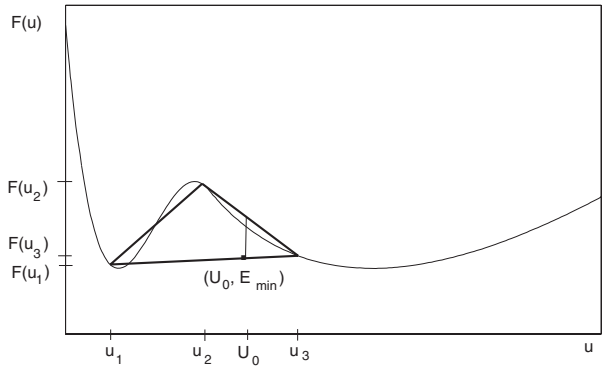

Figure 10. As in Fig. 9, but with $\lambda = \lambda_- < 0$.

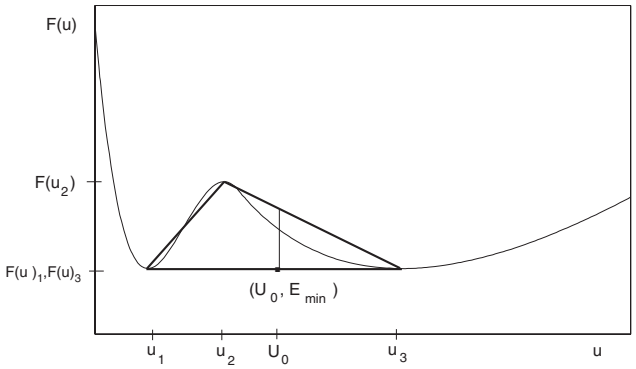

Figure 11. As in Fig. 9, but with $\lambda = 0$. If you compare the previous cases (Figs 9 and 10), it is clear that the minimum value of $E(u_0)$ for any u_0 occurs when the bottom line of the triangle connects the local minimums of the function.

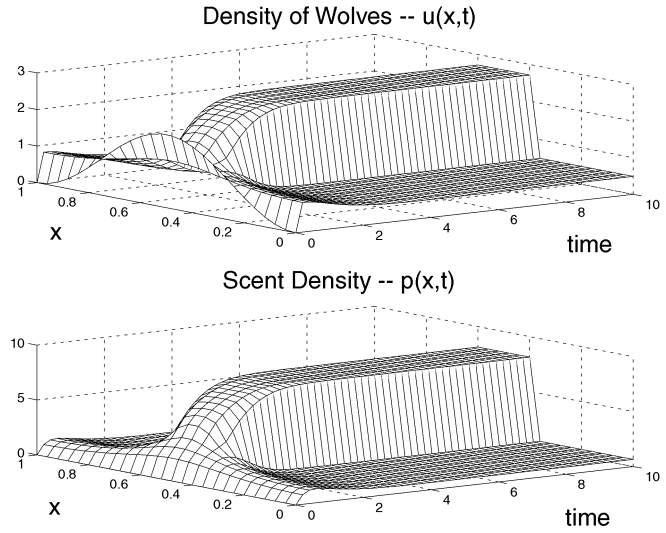

Figure 12. Beginning with a grouped distribution of wolves, a distinct region of high density marked by an abrupt change to lower densities emerges. The initial distribution of wolves was given by $1 - \cos(2\pi x)$. In this figure, the steady state values are $u_1 = 0.492$, $u_3 = 2.79$ which [from (30)] corresponds to $u/(1 + f(u)) = 0.298$ which is within 0.3% of the minimum energy constant C in (31). In this figure, $\epsilon = 0.1$.

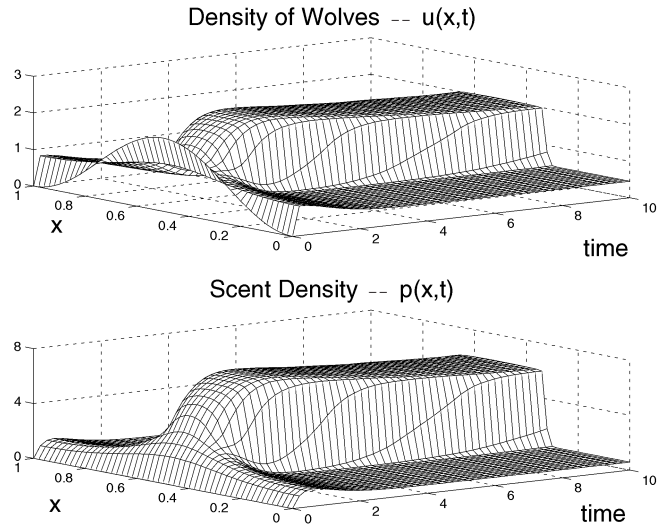

Figure 13. Starting with the same initial conditions as Fig. 12, we set $\sigma = 0.01$ which increases the range over which an individual can detect scent markings. The transition from low to higher densities is not so dramatic, which is consistent with the dispersion relation (see Fig. 4 and discussion in Section 6). In this figure, $\epsilon = 0.1$.

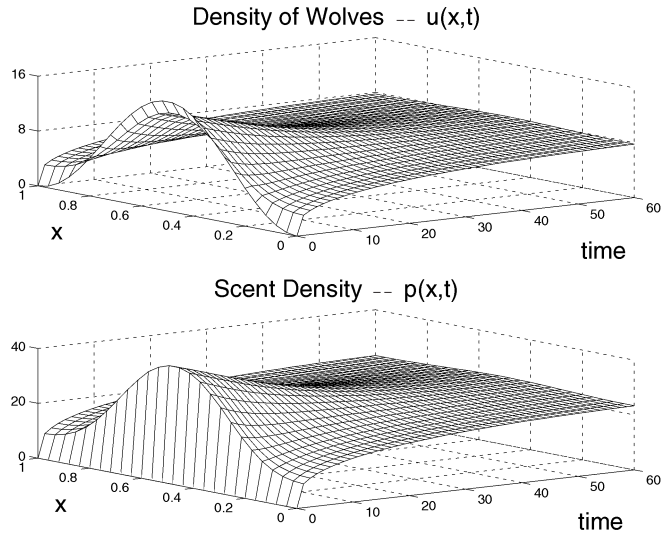

Figure 14. At higher densities, the solution moves toward a uniform distribution, $u = u_1$. In this figure $U_0 = 10.0$ and $\sigma = 0.01$.

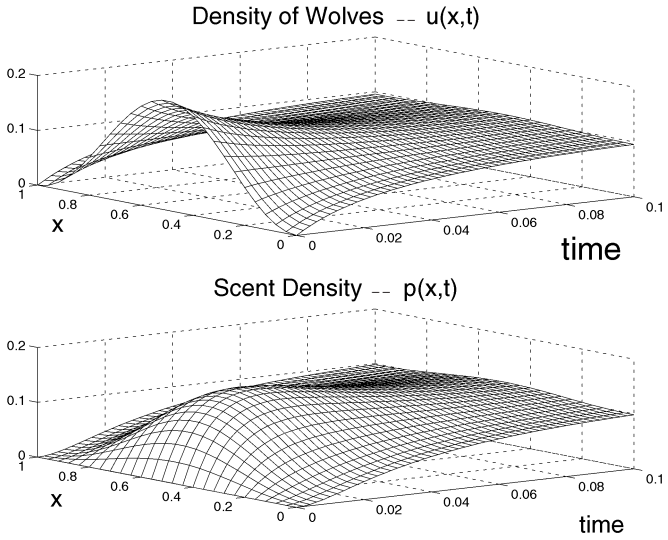

Figure 15. At lower densities, the solution very rapidly moves toward a uniform distribution, $u = u_1$. In this figure $U_0 = 0.1$ and $\sigma = 0.01$.

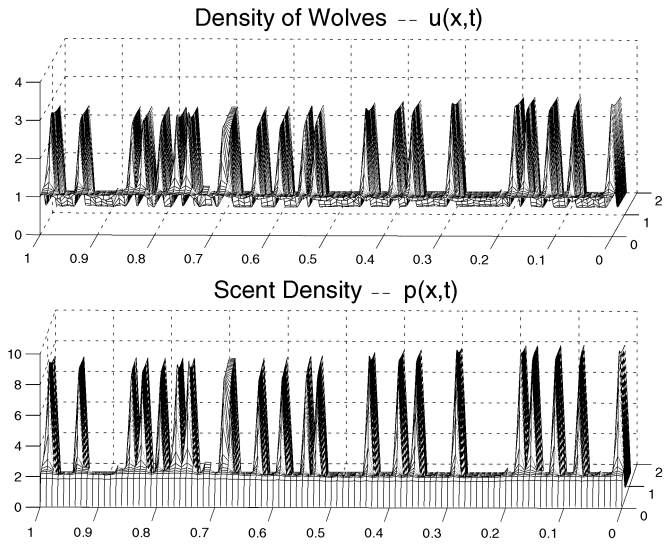

Figure 16. We begin here with an approximate uniform distribution with random perturbations, and $\sigma = 0$. Since perturbations of infinitely small wavelengths grow the fastest, there are many regions of high density separated by areas of low density. This simulation was executed with 100 spatial grid points. Our analysis suggests that as the number of grid points approaches ∞, these areas of higher density would become infinitely small. Simulations were also done with up to 1000 grid points, and match the analytical results. For this particular case, $u_3 = 2.84$ and $u_1 = 0.494$ which corresponds well with $u_3^* = 2.86$ and $u_1^* = 0.495$.

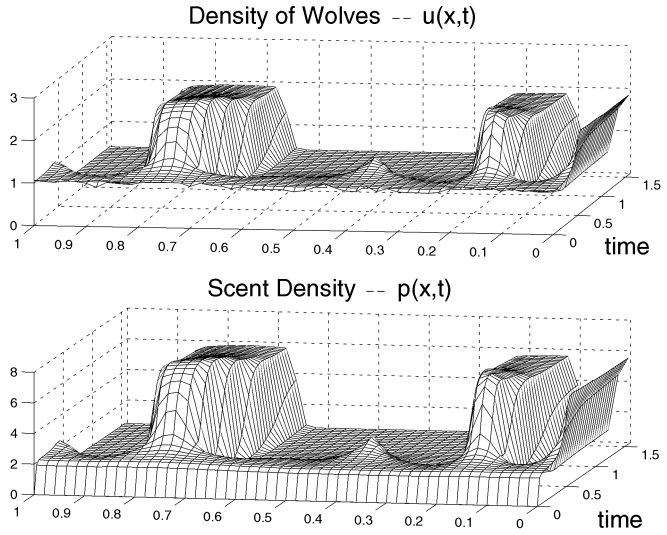

Figure 17. Starting with the same initial conditions as Fig. 16, we set $\sigma = 0.01$. Just as in Fig. 17, the difference is that transitions can no longer be so abrupt, and hence the computed solution does not have infinitely many areas of high density. It does, however, develop into two distinct areas of higher density. With different random perturbations, the solution can exhibit as many as four different areas of high density.

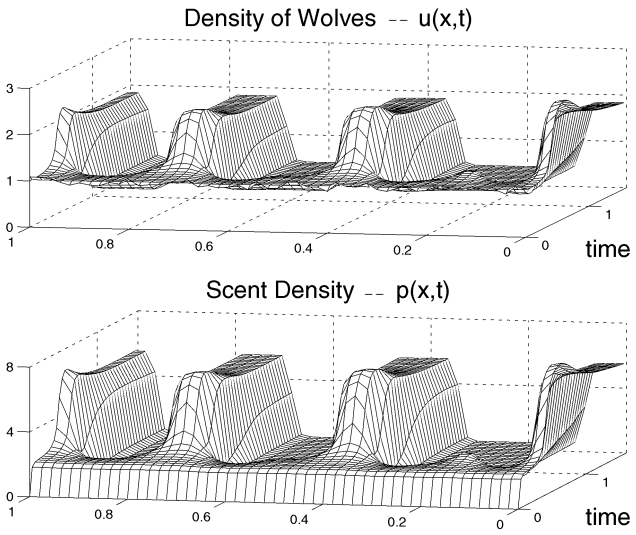

Figure 18. Starting with different random perturbations, this solution can exhibit four different areas of high density.

differencing (i.e., explicitly) and equations (21), (23) were solved using backward differencing (i.e., implicitly). In all simulations shown, we used 100 grid points in the x direction, which results in only very small differences from the same simulations done with 800 spatial grid points. Figures 12–18 were generated by down-sampling the amount of points used in both space and time.

It is evident from Figs 8 and 11 that the global energy minimum ($\lambda = 0$ and $u = u_1 = u_1^*$ on measure L_1, $u = u_3 = u_3^*$ on measure $1 - L_1$) can only be achieved when the normalized total number of wolves, U_0, lies between u_1^* and u_3^*. We chose parameter values as given in Appendix B, so that $u_1^* = 0.495$ and $u_3^* = 2.86$, as shown in Fig. 3. Except where noted, the value of ϵ was $\epsilon = 0.01$. The initial wolf density was given by $1 - \cos(2\pi x)$, with the normalized total number of wolves equal to $U_0 = 1.0$. The scent density was initially zero. The cases $\sigma = 0$ and 0.01 are shown in Figs 12 and 13, respectively. In Fig. 12, resulting steady state values $u_1 = 0.492$ and $u_3 = 0.279$ correlate closely with the u_1^* and u_3^* values given above. The differences are probably attributable to the fact that the global minimum energy analysis is valid only in the limit $\epsilon = 0$. We find that for nonzero initial conditions for scent density, the minimum energy level was not always achieved, although, equation (34) is always satisfied. This is a topic for further research.

The edge of the territory in Fig. 12, evidenced by the abrupt edge on the numerical simulation, is consistent with the dispersion relation shown in Fig. 5. When σ is nonzero the 'edges' on the simulation are rounded off and the u_1 and u_3 values are modified (Fig. 13).

When the normalized total wolf density exceeds u_3^*, the entire region becomes 'territory' (Fig. 14) and when the normalized wolf density is below u_1^* no territories

form (Fig. 15). For these cases it can be shown that the lowest energy solutions are spatially uniform solutions with $u = u_3 > u_1^*$, and $u = u_1 < u_1^*$, respectively.

When initial data are distributed randomly about a spatially uniform wolf density, the $\sigma = 0$ case gives an ill-behaved solution (Fig. 16), consistent with our analysis of Section 4.3. However, when $\sigma = 0.01$ the solution is no longer ill-behaved, but the location of the territory (or territories) depends upon the initial data (Figs 17 and 18). Although such randomly distributed initial data are not as biologically relevant as the grouped initial data that give rise to a single territory (Figs 12 and 13), we include these additional simulations to numerically illustrate the full range of model behavior.

7. DISCUSSION

We have shown that scent marking alone is sufficient to form a home range if there are two ingredients: (1) a propensity to remain near existing scent marks and (2) positive feedback, with increased scent marking in the presence of familiar scent marks. Each of these assumptions is supported by biological literature for wolves (see Introduction). Resulting home ranges are 'flat-topped' with abrupt edges. This model is most appropriate for sexually immature wolves that are in minimal contact with other packs.

The model in this paper contrasts with previous models which rely on pack interactions and existing den sites for territorial pattern formation. These other models modulate movement by the level of foreign scent marks, as opposed to familiar scent marks, and resulting territorial patterns show expected density gradually decreasing with distance from the den site (Lewis *et al*., 1997).

When there is no spatial averaging of scent information ($\sigma = 0$), our model is ill-posed, but once a small level of spatial averaging is included ($\sigma > 0$), the problem becomes well-posed. An analogous situation can be seen for an aggregation model proposed by Turchin (1989) [see also the discussion in Lewis (1994)]. Indeed our reduced model, given by equation (39), is Turchin's insect aggregation model, although derived by a different means. Thus the energy methods in this paper can be applied to models of aggregation more general than the formation of home ranges through scent marking.

Our model is, by necessity, simplistic—once home ranges are formed it is well known that 'cognitive maps' are used by canids to navigate around familiar areas (Peters, 1979), and we have not included this aspect. Furthermore, we assume that territorial scent marks are made by a single individual, or a single group of individuals moving together, such as an alpha pair. However, the modeling and analysis can be considered as a first step towards realistic spatially explicit models which include interactions with familiar scent marks.

ACKNOWLEDGEMENTS

This work was supported, in part, by a National Science Foundation grant DMS–9973212 (MAL) and by the Canada Research Chairs Program. Special thanks go to Markus Owen of Loughborough University, U.K., and David Eyre of the University of Utah who were kind enough to assist in the early development of this project. Comments from Paul Moorcroft and Thomas Hillen helped improve the manuscript.

APPENDIX A: FORWARD KOLMOGOROV EQUATION

We wish to derive the Fokker–Planck, or forward Kolmogorov equations from the assumptions in Section 2. We define $q(x, t)$ to be the probability density function of a wolf's location at time t. By the assumption that an individual can move at most a distance δx at each time step, we have that

$$\begin{aligned} q(x,t) = {} & R(x-\delta x, t-\delta t)q(x-\delta x, t-\delta t) \\ & + N(x, t-\delta t)q(x, t-\delta t) \\ & + L(x+\delta x, t-\delta t)q(x+\delta x, t-\delta t). \end{aligned}$$

What this says is that in order to be at point x at time t then an individual at time $t-\delta t$ was either at $x-\delta x$ and moved to the right, $x+\delta x$ and moved to the left, or at x, and did not move during that time step. In doing this, we have also used the assumption that probability of moving is independent of everything besides local scent density. Using (2), we can rewrite $q(x, t)$ in terms of $N(x, t)$ as

$$\begin{aligned} q(x,t) = {} & \frac{1-N(x-\delta x, t-\delta t)}{2} q(x-\delta x, t-\delta t) \\ & + N(x, t-\delta t)q(x, t-\delta t) \\ & \frac{1-N(x+\delta x, t-\delta t)}{2} q(x+\delta x, t-\delta t). \end{aligned}$$

Now, in order to simplify this, we do a power series expansion of all terms involving either δt or δx. After doing this, and putting all terms that include δt on the left-hand side of the equal sign, we are left with

$$\delta t q_t = \left(\frac{\delta x^2}{2}\right)\left(\frac{\partial^2}{\partial x^2}[(1-N(x,t))q(x,t)]\right) + \text{ h.o.t.} \tag{A1}$$

We take the limit as δx and $\delta t \to 0$ in such a way that

$$\lim_{\delta x \to 0} \lim_{\delta t \to 0} \frac{\delta x^2}{2\delta t} = D_0.$$

This is called the diffusion limit, and has been commonly used to derive diffusion-related equations. Another advantage in doing this is that the higher order terms in the equation all go to zero. If we now define $u(x,t) = u_0 q(x,t)$ to be the expected wolf density, what we are now left with is

$$\frac{\partial u}{\partial t} = \frac{\partial^2}{\partial x^2}[D_0(1 - N(x,t))u(x,t)] \tag{A2}$$

which is (3).

APPENDIX B: THE FUNCTION $m(p)$

$$m(p) = \begin{cases} ap & 0 \le p \le \frac{b}{a} \\ b & p \ge \frac{b}{a} \end{cases} \tag{B1}$$

$$m(p) = \begin{cases} ap & 0 \le p \le \frac{b}{a} \\ \frac{a^2}{b}p^2 + \frac{5a}{2}p - \frac{9b}{16} & \frac{3b}{4a} \le p \le \frac{5b}{4a} \\ b & p \ge \frac{5b}{4a} \end{cases}. \tag{B2}$$

In the simulations, we took the following values for various parameters:

$$\gamma = 1 \qquad \mu = 1 \qquad \alpha = 1$$

$$a = 0.5 \qquad b = 2 \qquad D = 1.$$

APPENDIX C: THE FUNCTIONS $f(u)$ AND $\phi(u)$

We define $f(u)$ and $\phi(u)$ for each particular case of $m(p)$ as follows: for the piecewise linear $m(p)$ (B1)

$$f(u) = \begin{cases} \frac{u}{1+\frac{u}{2}} & 0 \le u \le \frac{4}{3} \\ \frac{u}{1+3u} & u \ge \frac{4}{3} \end{cases} \tag{C1}$$

$$\phi(u) = \begin{cases} \frac{u(2-u)}{2+u} - C & 0 \le u \le \frac{4}{3} \\ \frac{u}{1+3u} - C & u \ge \frac{4}{3}. \end{cases} \tag{C2}$$

For the piecewise quadratic $m(p)$ (B2)

$$f(u) = \begin{cases} \frac{u}{1+\frac{u}{2}} & 0 \le u \le \frac{6}{5} \\ \frac{5u-4+2\sqrt{6u^2-10u+4}}{u} & \frac{6}{5} \le u \le \frac{5}{3} \\ \frac{u}{1+3u} & u \ge \frac{5}{3} \end{cases} \tag{C3}$$

$$\phi(u) = \begin{cases} \frac{u(2-u)}{2+u} - C & 0 \le u \le \frac{6}{5} \\ \frac{u^2}{6u-4+2\sqrt{6u^2-10u+4}} - C & \frac{6}{5} \le u \le \frac{5}{3} \\ \frac{u}{1+3u} - C & u \ge \frac{4}{3}. \end{cases} \tag{C4}$$

REFERENCES

Aronson, D. G. (1985). The role of diffusion in mathematical population biology: Skellam revisited, in *Mathematics in Biology and Medicine*, V. Capaso, E. Grosso and S. L. Paveri-Fontana (Eds), Berlin: Springer-Verlag, pp. 2–6.

Lewis, M. A. (1994). Spatial coupling of plant and herbivore dynamics: the contribution of herbivore dispersal to transient and persistent "waves" of damage. *Theor. Popul. Biol.* **45**, 277–312.

Lewis, M. A. and J. D. Murray (1993). Modelling territoriality and wolf–deer interactions. *Nature* **366**, 738–740.

Lewis, M. A., K. A. J. White and J. D. Murray (1997). Analysis of a model for wolf territories. *J. Math. Biol.* **35**, 749–774.

Mech, D. L. (1991). *The Way of The Wolf*, Stillwater, MN: Voyageur Press.

Merti-Millhollen, A. S., P. A. Goodmann and E. Klinghammer (1986). Wolf scent marking with raised-leg urination. *Zoo Biol.* **5**, 7–20.

Moorcroft, P. R., M. A. Lewis and R. L. Crabtree (1999). Analysis of coyote home ranges using a mechanistic home range model. *Ecology* **80**, 1656–1665.

Murray, J. D. (1989). *Mathematical Biology*, *Biomathematics* **19**, Berlin: Springer-Verlag.

Okubo, A. (1980). *Diffusion and Ecological Problems: Mathematical Models*, *Biomathematics* **10**, Berlin: Springer-Verlag.

Parrish, S. (1998). Analysis of a home range model: pattern formation from scent-marking, Master's thesis, University of Utah.

Peters, R. P. (1974). Wolf sign: scents and space in a wide-ranging predator, PhD thesis, University of Michigan, Ann Arbor, MI.

Peters, R. P. (1979). Mental maps in wolf territoriality, in *The Behavior and Ecology of Wolves*, E. Klinghammer (Ed.), New York, NY: Garland Press, pp. 119–152.

Peters, R. P. and L. D. Mech (1975). Scent marking in wolves. *Am. Scientist* **63**, 628–637.

Rothman, R. J. and L. D. Mech (1979). Scent-marking in lone wolves and newly formed pairs. *Anim. Behav.* **27**, 750–760.

Turchin, P. (1989). Population consequences of aggregative movement. *J. Anim. Ecol.* **58**, 75–100.

White, K. A. J., M. A. Lewis and J. D. Murray (1996). A model for wolf-pack territory formation and maintenance. *J. Theor. Biol.* **178**, 29–43.

White, K. A. J., M. A. Lewis and J. D. Murray (1998). *On Wolf Territoriality and Deer Survival*, Chap. 6, Springer Verlag, pp. 105–126.

Received 6 May 2001 and accepted 28 October 2001